Defect reduction in overgrown semi-polar (11-22) GaN on a regularly arrayed micro-rod array template

Y. Zhang, J. Bai, Y. Hou, R. M. Smith, X. Yu, Y. Gong, and T. Wang

Citation: AIP Advances **6**, 025201 (2016); doi: 10.1063/1.4941444
View online: http://dx.doi.org/10.1063/1.4941444
View Table of Contents: http://aip.scitation.org/toc/adv/6/2
Published by the American Institute of Physics

Defect reduction in overgrown semi-polar (11-22) GaN on a regularly arrayed micro-rod array template

Y. Zhang, J. Bai, Y. Hou, R. M. Smith, X. Yu, Y. Gong, and T. Wang[a]
Department of Electronic and Electrical Engineering, University of Sheffield, Mappin Street, Sheffield, S1 3JD, United Kingdom

(Received 23 November 2015; accepted 21 January 2016; published online 2 February 2016)

We demonstrate a great improvement in the crystal quality of our semi-polar (11-22) GaN overgrown on regularly arrayed micro-rod templates fabricated using a combination of industry-matched photolithography and dry-etching techniques. As a result of our micro-rod configuration specially designed, an intrinsic issue on the anisotropic growth rate which is a great challenge in conventional overgrowth technique for semi-polar GaN has been resolved. Transmission electron microscopy measurements show a different mechanism of defect reduction from conventional overgrowth techniques and also demonstrate major advantages of our approach. The dislocations existing in the GaN micro-rods are effectively blocked by both a SiO_2 mask on the top of each GaN micro-rod and lateral growth along the *c*-direction, where the growth rate along the *c*-direction is faster than that along any other direction. Basal stacking faults (BSFs) are also effectively impeded, leading to a distribution of BSF-free regions periodically spaced by BSF regions along the [-1-123] direction, in which high and low BSF density areas further show a periodic distribution along the [1-100] direction. Furthermore, a defect reduction model is proposed for further improvement in the crystalline quality of overgrown (11-22) GaN on sapphire.
[http://dx.doi.org/10.1063/1.4941444]

The major achievement in the field of III-nitride semiconductors made so far are mainly limited to c-plane GaN grown on (0001) sapphire, represented by high brightness InGaN/GaN based blue emitters. However, this polar orientation generates a number of fundamental issues, preventing further development in the field of III-nitride semiconductors, in particular, long wavelength optoelectronics. For instance, a strong piezoelectric-field induced polarization effect as a result of InGaN/GaN emitters grown along the polar direction leads to a reduction in overlap between electron and hole wavefunctions and thus a reduced quantum efficiency.[1–3] This becomes more severe when emitters move toward longer wavelengths, such as the green and yellow spectral region, generating so-called "green/yellow" gap issue. A further greater barrier to overcoming the "green/yellow" gap is due to an extreme difficulty in enhancing indium incorporation into GaN due to the large lattice mismatch and miscibility between InN and GaN. One clear way forward, meeting the fundamental challenges, is to grow along a semi-polar direction, in particular, [11-22] direction. It has been predicted that (11-22) surface leads to easier accommodation of larger indium atoms than either polar- or non-polar surface,[4] favoring the growth of high indium content InGaN layers which are necessary for green or yellow emitters.

Currently, the major challenge is due to the crystalline quality of semi-polar GaN, which is far from satisfactory. So far, semi-polar GaN with device performance is exclusively grown on free-standing semi-polar GaN substrates, which are obtained by slicing very thick c-plane GaN along semi-polar orientations. This limits the substrate size to a square of 10×10 mm^2 (ref.5–7), and thus is extremely expensive. Therefore, it would be impractical for industry.

[a]Author to whom all correspondence should be addressed; E-mail: t.wang@sheffield.ac.uk

There is a limited number of reports on overgrowth of semi-polar GaN mainly based on conventional epitaxial lateral overgrowth (ELOG)[8–13] which generally leads to a non-uniformity issue and requests a thick overgrown layer (typically > 10 μm) in order to achieve an atomically flat surface. In order to address these issues, previously we reported an overgrowth approach based on self-organised nickel nano-masks, leading to a significant improvement in the crystal quality of either semi- or non- polar GaN on sapphire and achieving an atomically flat surface with an overgrown layer of only a few micrometers.[14,15] Very recently, we have developed another cost-effective approach to the overgrowth of semi-polar GaN on mask-patterned micro-rod arrays on 2“ sapphire, where the diameter of micro-rods with a regular patterning can be accurately controlled. On such high quality semi-polar GaN templates, we have achieved high performance semi-polar light emitting diodes (LEDs) with a wide spectral range of up to amber.[16,17]

In this letter, we investigate in detail a mechanism of the defect reduction in the overgrown semi-polar (11-22) GaN on the regular micro-rod array templates by transmission electron microscopy (TEM) measurements, and a detailed model has been established, essentially allowing us to further improve the crystalline quality of overgrowth semi-polar GaN on sapphire.

A single (11-22) GaN layer with a thickness of 1.3 μm is grown on *m*-plane sapphire using our high temperature AlN buffer by metal organic chemical vapor deposition (MOCVD).[18] For subsequent overgrowth, mask-patterned micro-rod arrays have been fabricated on the semi-polar GaN layer. Firstly, a 500 nm SiO_2 layer is deposited by plasma enhanced chemical vapor deposition (PECVD), followed by a standard photolithography patterning process and subsequent dry etching processes using Inductively Reactive Plasma (ICP) and Reactive Ion Etching (RIE) techniques. Regularly arrayed SiO_2 micro-rods can be achieved. Finally, the SiO_2 micro-rods served as a second mask are used to etch the GaN underneath in order to form regularly arrayed GaN micro-rods with the SiO_2 remaining on their top. The micro-rod masks with different diameters from 1.5 to 3 μm have been employed for the fabrication of micro-rod array templates. As an example, Figure 1(a) shows a top-view scanning electron microscope (SEM) image of a micro-rod array template with a diameter of 3.5 μm and a spacing (edge to edge along [1-100] direction or [-1-123] direction) of

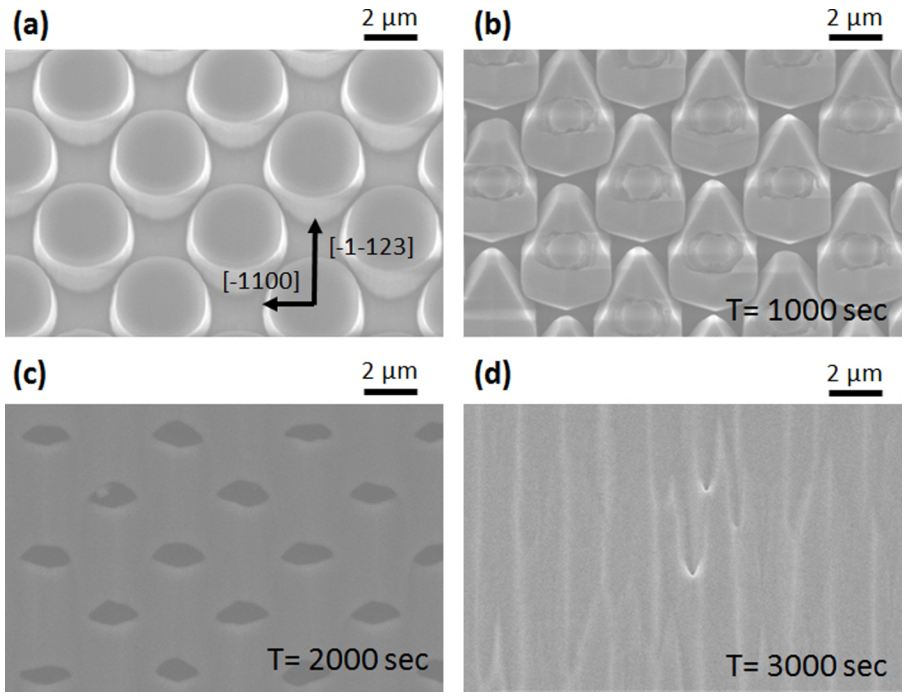

FIG. 1. (a) Top-view SEM image of micro-rod arrays with a diameter of 3.5 μm and spacing (edge to edge) of 2 μm; (b)-(d) SEM images of the surface morphology of our (11-22) GaN with overgrowth time of 1000, 2000 and 3000 seconds, respectively.

2 μm. The subsequent overgrowth process is carried out by MOCVD with a growth temperature, V/III ratio and pressure at 1120°C, 1600 and 75 Torr, respectively. Please note that the approach is fundamentally different from our previous method based on self-organised nickel nanomasks,[15] where the rod diameter, the shape, the spacing between rods and the orientation of the rod arrays are all randomly distributed. Due to anisotropic growth rates of semi-polar GaN, it would be necessary to maximize the spacing along one particular direction (for example, the projection of *c*-direction to the surface), and minimize the spacing along another direction (for example, *m*-direction). These can be achieved only by the present approach. Furthermore, due to an accurate control in the orientation of micro-rod arrays using the present approach, it is expected that the defect reduction mechanism is different from that for the previous self-organized nickel nano-mask approach.

Figure 1(b)-1(d) show an evolution of the surface morphology of the overgrown layer on an initial growth stage, demonstrating a change in surface morphology when the growth time is 1000, 2000 and 3000 seconds, respectively. The overgrowth initiates from the exposed sidewalls of micro-rods as shown in Figure 1(b), and the lateral growth is dominated by the growth along the [0001] direction labelled as *c*-direction and the [11-20] direction labelled as *a*-direction. Comparing the lengths of the two growing wings, the *c*-direction growth is faster than the *a*-direction growth. Moreover, the growth along the [-1100] direction labelled as *m*-direction is negligible. After the coalescence of the *c*-direction growth and the *a*-direction growth facets, the GaN growth tends to move upward. When the thickness of the overgrown layer exceeds the height of the micro-rods, the growth begins to extend to cover the SiO_2 masks. Although the *m*-direction growth is slower than the growth along other directions, the specially designed pattern of the micro-rods as shown in Figure 1(a) compensates the anisotropic growth rate, also facilitating another second coalescence occurring over the SiO_2 masks. Eventually a full coalescence is achieved. A smooth surface can be achieved with the overgrowth of about 4 μm, which is faster than any other conventional ELOG techniques.[19,20] Initial X-ray diffraction (XRD) measurements have been performed as a function of azimuth angle, exhibiting that the full width at half maximum (FWHM) of on-axis XRD rocking curves measured along the [1-100] and [-1-123] directions is 320 and 260 arcsec, respectively. These represent the best results on semi-polar GaN with a similar thickness grown on sapphire.

The specimens for both cross-sectional and plan-view transmission electron microscopy (TEM) measurements are prepared by initial mechanical lapping/polishing and then ion milling down to electron transparency. TEM measurements have been performed using a Philips EM430 TEM operating at 200 kV. Based on an invisibility criterion,[20–24] dislocations are out of contrast when the product of a diffraction vector $\boldsymbol{g}$ and a dislocation displacement vector $\boldsymbol{R}$ equals zero, namely, $\boldsymbol{g} \cdot \boldsymbol{R}=0$ (It would still be possible to observe a weak contrast of dislocations for a very thin specimen in the case of the dislocation unparalleled to its burger vector. This does not apply in our case.); and stacking faults are invisible when the product is an integer, including zero.

Figure 2(a) shows a typical bright-field cross-sectional TEM image taken along [1-100] zone-axis with $\boldsymbol{g}$=0002, indicating **c**-type threading dislocations (TDs), **a**+**c** TDs and Shockley partial dislocations; while Figure 2(b) shows a typical bright-field cross-sectional TEM image taken along [1-100] zone-axis but with $\boldsymbol{g}$=11-20, demonstrating **a**-type TDs, **a**+**c** TDs and Frank partial dislocations. Figure 2(a) and 2(b) show all kinds of the dislocations, demonstrating that the dislocations (with an inclination angle of 58.4° to surface) from the GaN micro-rods under the SiO_2 masks have been greatly reduced as a result of the overgrowth on our micro-rod arrays.

The voids in a triangular shape observed in the trenches between the micro-rods are formed as a result of the first coalescence of the *c*-direction growth facets and the *a*-direction growth facets from two neighboring micro-rods. The voids extend from the sapphire substrate, confirming that the growth initiates from the exposed sidewalls rather than the bottom of the trenches between micro-rods. It is important because the GaN growth from the bottom needs to be suppressed in order to prevent the defects penetrating from the micro-rods to the overlying structures. Similar to the other overgrowth techniques, the GaN grown laterally along the *c*-direction exhibits approximately free of dislocations, whereas the GaN grown along the *a*-direction contains a number of defects.[12,22] Due to the fact that the *c*-direction growth rate is faster than the *a*-direction growth rate, the *a*-direction growth is eventually stopped by the *c*-direction growth, terminating the propagation of defects from the *a*-direction growth. Therefore, the growth conditions favoring the c-facet growth

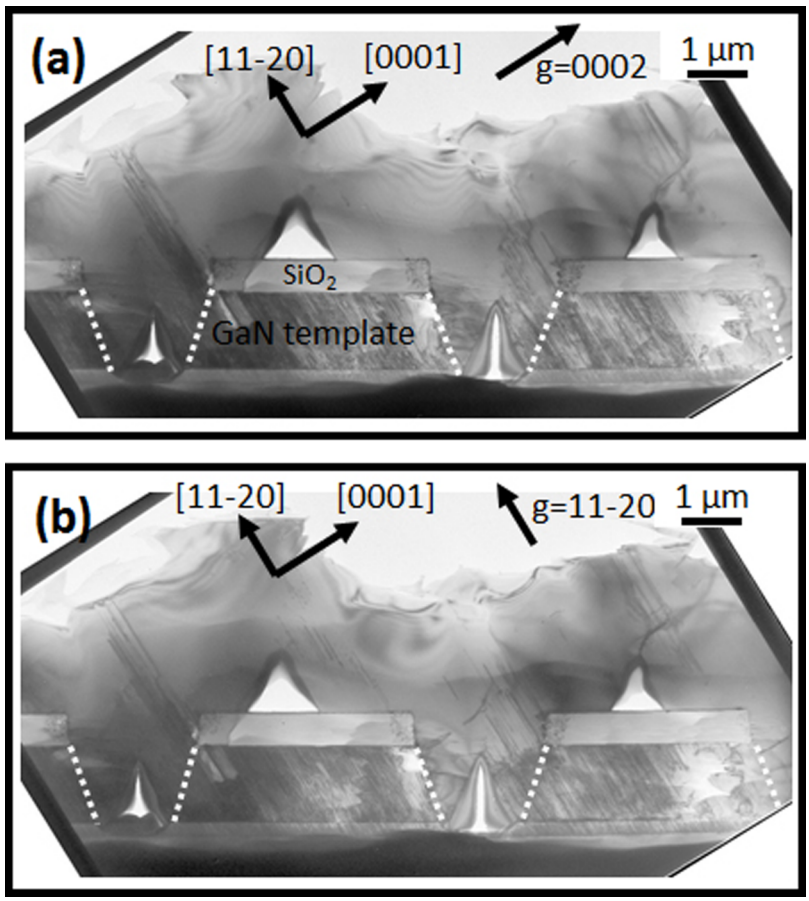

FIG. 2. Bright field cross-sectional TEM images of our overgrown GaN layer taken along the [1-100] zone-axis under a diffraction vector of (a) g=0002 and (b) g=11-20.

are preferred on the early overgrowth stage, leading to an efficient reduction in dislocations and extended defects. As a result, the majority of the pre-existing dislocations in the GaN micro-rods are effectively prevented from penetrating by both the SiO_2 masks and the c-direction growth. Only a small part of the dislocations along the *a*-direction propagate to the surface. Furthermore, another kind of voids have also been observed over the SiO_2 mask on the top of each micro-rod as a consequence of the second coalescence along the [-12-10] and [2-1-10] directions as well. It is worth noting that a very small number of extra dislocations are generated due to the 2nd coalescence. Our plan-view TEM image indicates that the overall dislocation density in our overgrown (11-22) semi-polar GaN is about 4.2×10^8 cm^{-2}, demonstrating a significant reduction in dislocation density from the order of 10^{10} cm^{-2} in the as-grown GaN which is used to fabricate into the micro-rod array template.

Basal stacking faults (BSFs), as extended defects, can be observed along either the [-12-10] or the [2-1-10] zone-axis by tilting 30° from the [1-100] zone-axis.[23] Figure 3(a) shows a typical bright-field cross-sectional TEM image taken along the [2-1-10] direction with $\boldsymbol{g}$=1-100, where BSFs appear as straight dark lines with an inclination angle of 58.4° to the surface. Since the BSFs exist in basal planes, they are impeded by the *c*-direction growth. As denoted by the red arrows in Figure 3(a), part of the BSFs along the *a*-direction are blocked by the adjacent c-direction growth (leading to defect-free regions), which are terminated very likely in the form of PDs and prismatic stacking faults (PSFs), while the rest of the BSFs along the *a*-direction are found to survive from the first coalescence process and propagate to the surface. This forms the free-BSF regions and the BSF regions distributing in a periodic form along the [-1-123] direction. What also interests us is the appearance of the BSF clusters over the SiO_2 masks, as marked by the blue arrows in Figure 3(a).

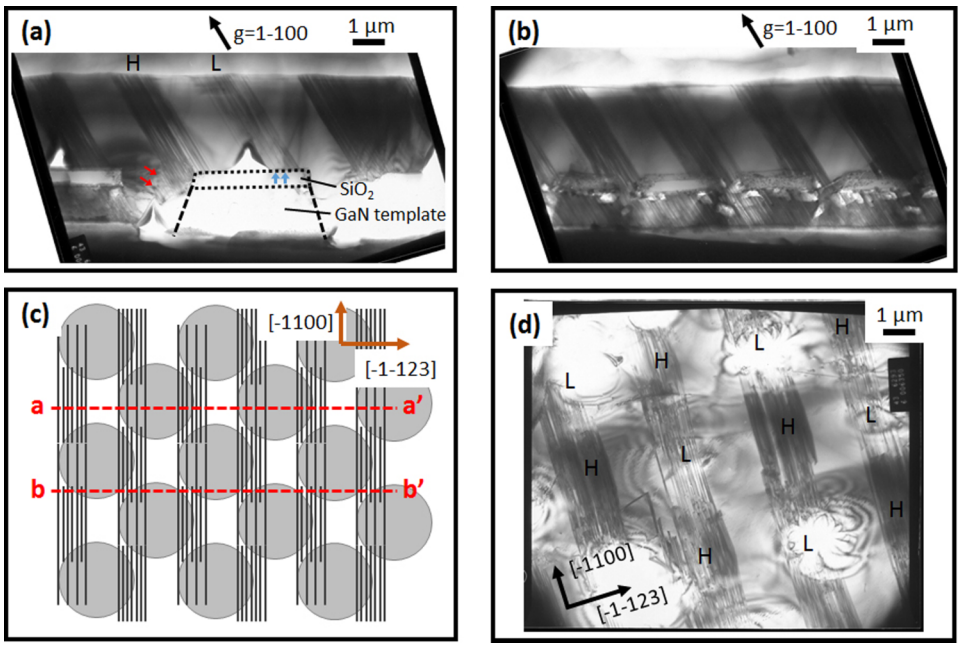

FIG. 3. (a) and (b) Bright-field cross-sectional TEM images of our (11-22) overgrown GaN layer viewed along the [11-20] zone-axis with diffraction vector **g**=1-100, but with preparing specimens cleaved differently; (c) Schematic diagrams of the BSF distribution on the sample surface and our micro-rod patterning. The dash lines labeled as a-a' and bb' depict the different cleavage directions for preparing the specimens from a same sample used for TEM observation as shown (a) and (b), respectively; (d) Plan-view TEM image of our (11-22) overgrown GaN with a diffraction vector **g**=1-100.

To study the origin of these unexpected BSFs, a TEM specimen was particularly prepared by cleaving along a direction schematically illustrated by a dash line labelled as b-b' as shown in Figure 3(c). Figure 3(c) also schematically show a distribution of BSFs indicated by the vertical dark lines, which will be explained later. In this case, all the micro-rods belonging to the two neighbouring rows can be observed in a cross-sectional TEM image as shown in Figure 3(b), while the upper and lower voids cannot be observed. By comparing Figure 3(a) and 3(b), it can be concluded that the BSF clusters observed on the left side of the SiO_2 masks on each micro-rod in Figure 3(a) are from a different micro-rod on a neighbouring row. One solid evidence is that the spacing between these BSF clusters is around 1.5 μm, similar to the distance in Figure 3(a) with the cleavage along micro-rod centre to centre, namely, along a dash line marked as a-a' in Figure 3(c). This is also confirmed by the plan-view TEM image in Figure 3(d).

Figure 3(d) clearly demonstrates that BSF clusters with orientation along the *m*-direction, i.e., [-1100], are separated by defect-free regions along the [-1-123] direction. The width of the defect-free areas is around 1.5 μm, consistent with the cross-sectional TEM images as shown in Figure 3(a). In addition, the distribution of these BSF clusters shows a repeat of high BSF density areas (labelled with H) and low BSF density areas (labelled with L). It means the BSFs can expand within the basal plane, propagating with a component parallel to the *m*-direction during the overgrowth above the SiO_2 masks. During the second coalescence process, some BSFs are terminated by a formation of either PDs or PSFs, leading to a further reduction in BSF density.[24] Consequently, this forms one area with a low BSF density (i.e., L region) and another area with a high BSF density (i.e., H region), appearing in a periodic form along the *m*-direction.

It is worth noting that the locations of the defect-free regions and defect regions depend on layer thickness as schematically shown in Figure 3(c), as the defects penetrate along the *a*-direction which is 58° with respect to the surface. Our plan-view TEM image shows that the average BSF density of our overgrown GaN on a 3.5 μm micro-rod template has been reduced to 4.7×10^4 cm^{-1}.

In order to further optimize the design of our micro-rod mask patterning, a model has been built up to understand the influence of the micro-patterning on defect reduction. Figure 4(a)

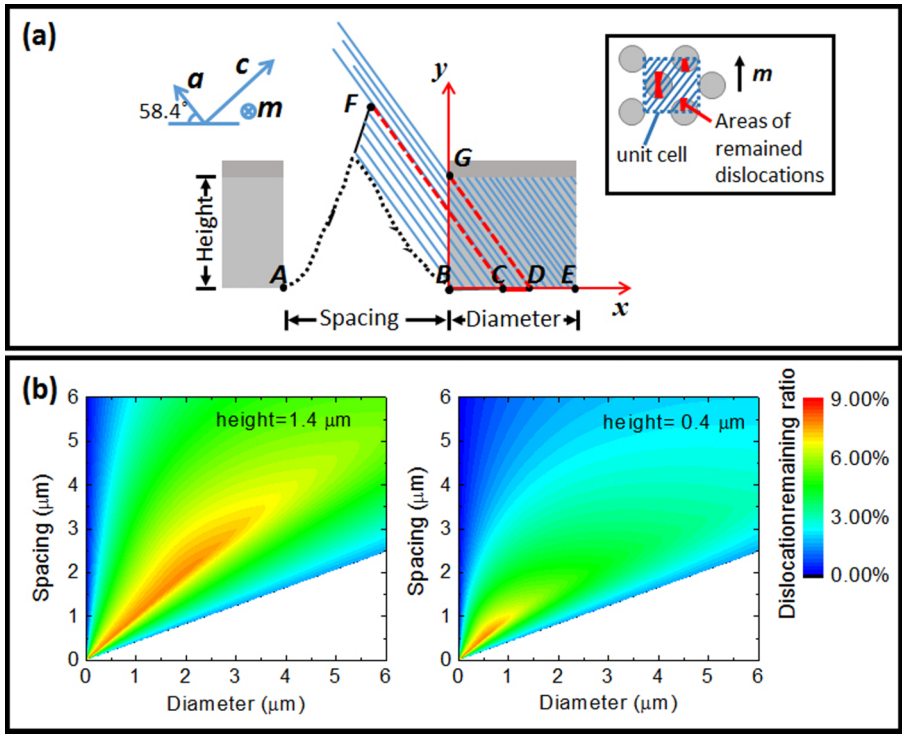

FIG. 4. (a) Schematic diagram of our dislocation reduction model for (11-22) semi-polar overgrown GaN on micro-rod arrays along the [1-100] direction. (b) Contour plots of the dislocation remaining ratio as a function of micro-rod diameter and micro-rod spacing with a micro-rod height of 1.4 and 0.4 μm, respectively.

schematically illustrates a cross-sectional diagram of micro-rods along the *m* direction. Segment **AE** represents one period. Based on the TEM observations above, only the dislocations located in the line segment **CD** (marked by red line) have a chance to propagate to the surface, while other dislocations are blocked either during the first coalescence (line segment **BC**) or by the SiO_2 masks (line segment **DE**). Point C and D are the projections of the top point F of the first coalescence front and the top point G of the sidewall of a micro-rod onto sapphire surface along the *a*-direction, respectively. By integrating the line segment **CD** along the *m*-direction, an area where dislocations have a chance to propagate to the surface is obtained (as illustrated by the inset of Figure 4(a)). The ratio of this area to the area of integrated line segment **AE** along the *m*-direction can be treated as a dislocation remaining ratio. For simplicity, any decrease in dislocation density due to the lateral overgrowth along the *a*-direction and a very small number of extra dislocations generated during the coalescence processes[11,25] are not taken into account. Figure 4(b) shows our simulation result, describing the relationship between the dislocation remaining ratio and micro-rod diameter & spacing between micro-rods, where the height of micro-rods is set as 0.4 and 1.4 μm as two examples, respectively. In both cases as shown in Figure 4(b), our simulation is limited to a diameter of micro-rods of below 6 μm, as it would be difficult to achieve an atomically flat surface if overgrown on micro-rods with a larger diameter. In Figure 4(b), the blue area represents a low dislocation remaining ratio while the red area represents a high ratio. There are two low-ratio areas; one is the upper-left corner with a very small micro-rod diameter of below 0.5 μm, and the other one is in the lower-right with a micro-rod diameter of a few micrometers and a micro-rod spacing from 1.5 to 2.5 μm. A conventional photolithography typically uses an ultraviolet lighting source with a wavelength of ~300 nm, and thus it would be difficult to fabricate rod arrays with a sub-micron diameter. Consequently, it is worth paying attention to the lower-right blue area, where both micro-rod diameter and micro-rod spacing are on a few micrometer scale. By carefully examining Figure 4(b), the range for the blue area increases when the micro-rod height reduces from 1.4 to 0.4 μm, enhancing the chance for tuning either micro-rod diameter or micro-rod spacing

for effectively blocking defect penetration. On the other hand, this also demonstrates that a decrease in the height of micro-rods potentially leads to a further reduction in dislocation density. It has been confirmed by our very recent experiments which show better crystal quality in the semi-polar GaN overgrown on the micro-rods with a height of 0.4 μm compared to the micro-rods with a height of 1.4 μm. A reduction in micro-rod height leads to a decrease in the exposed areas of the sidewalls of the micro-rods for the growth along the *a*-direction which is beneficial for the defect reduction.

In conclusion, the defect reduction in the overgrown semi-polar (11-22) GaN on regularly arrayed micro-rod arrays has been studied by TEM measurements. It has been found that the majority of the dislocations and BSFs are blocked by the SiO_2 masks and the coalescence processes during the overgrowth. Owing to the faster growth rate along the *c*-direction than along the *a*-direction, the defects from the growth along the *a*-direction are effectively blocked by the growth along the *c*-direction (the *c*-direction growth leads to free-defect). In addition, the BSFs have been found to expand within the basal planes, propagating with a component parallel to the *m*-direction. After the second coalescence over the SiO_2 masks, the BSFs distribute in a periodic form consisting of defect-free regions and defect regions along the [-1-123] direction, where the defect regions compose of low density BSF clusters and high density BSF clusters in a periodic form along the *m*-direction.

ACKNOWLEDGMENT

Financial support is acknowledged from the EPSRC, UK via Grant No. EP/M015181/1, "Manufacturing nano-GaN", and Seren Photonics Ltd.

[1] F. Bernardini, V. Fiorentini, and D. Vanderbilt, Phys. Rev. B **56**, R10024 (1997).
[2] P. Waltereit, O. Brandt, A. Trampert, H. T. Grahn, J. Menniger, M. Ramsteiner, M. Reiche, and K. H. Ploog, Nature (London) **406**, 865 (2000).
[3] T. Takeuchi, H. Amano, and I. Akasaki, Jpn. J. Appl. Phys. Part 1 **39**, 413 (2000).
[4] J E Northrup, Appl. Phys. Lett **95**, 133107 (2009).
[5] P. Fini, L. Zhao, B. Moran, M. Hansen, H. Marchand, J. P. Ibbetson, S. P. DenBaars, U. K. Mishra, and J. S. Speck, Appl. Phys. Lett. **75**, 1706 (1999).
[6] K. Hiramatsu, K. Nishiyama, M. Onishi, H. Mizutani, M. Narukawa, A. Motogaito, H. Miyake, Y. Iyechika, and T. Maeda, J. Cryst. Growth **221**, 316 (2000).
[7] H Masui, S Nakamura, S P DenBaars, and U K Mishra, IEEE Transactions on Electron Devices **57**, 88 (2010).
[8] Y. Yoshizumi, M. Adachi, Y. Enya, T. Kyono, S. Tokuyama, T. Sumitomo, K. Akita, T. Ikegami, M. Ueno, K. Katayama, and T. Nakamura, Appl. Phys. Express **2**, 092101 (2009).
[9] H. Zhong, A. Tyagi, N. N. Fellows, R. B. Chung, M. Saito, K. Fujito, J. S. Speck, S. P. DenBarrs, and S. Nakamura, Electron. Lett. **43**, 825 (2007).
[10] I. Kidoguchi, A. Ishibashi, G. Sugahara, and Y. Ban, Appl. Phys. Lett. **76**, 3768 (2000).
[11] B. Imer, F. Wu, S. P. DenBaars, and J. S. Speck, Appl. Phys. Lett. **88**, 061908 (2006).
[12] X. Ni, Ü. Özgür, A. A. Baski, H. Morkoç, L. Zhou, D. J. Smith, and C. A. Tran, Appl. Phys. Lett. **90**, 182109 (2007).
[13] D. Iida, M. Iwaya, S. Kamiyama, H. Amano, and I. Akasaki, J. Cryst. Growth **311**, 2887 (2009).
[14] K. Xing, Y. Gong, J. Bai, and T. Wang, Appl. Phys. Lett. **99**, 181907 (2011).
[15] J. Bai, Y. Gong, K. Xing, X. Yu, and T. Wang, Appl. Phys. Lett. **102**, 101906 (2013).
[16] Y. Gong, K. Xing, B. Xu, X. Yu, Z. Li, J. Bai, and T. Wang, ECS Transactions **66**, 151 (2015).
[17] J. Bai, B. Xu, F. G. Guzman, K. Xing, Y. Gong, Y. Hou, and T. Wang, unpublished.
[18] T. Wang, K. B. Lee, J. Bai, P. J. Parbrook, R. J. Airey, Q. Wang, G. Hill, F. Ranalli, and A. G. Cullis, Appl. Phys. Lett. **89**, 081126 (2006).
[19] P. de Mierry, N. Kriouche, M. Nemoz, and G. Nataf, Appl. Phys. Lett. **94**, 191903 (2009).
[20] N. Kriouche, P. Vennéguès, M. Nemoz, G. Nataf, and P. de Mierry, J. Cryst. Growth **312**, 2625 (2010).
[21] T. Hino, S. Tomiya, T. Miyajima, K. Yanashima, S. Hashimoto, and M. Ikeda, Appl. Phys. Lett. **76**, 3421 (2000).
[22] P. Vennéguès, Semicond. Sci. Technol. **27**, 024004 (2012).
[23] F. Wu, Y. D. Lin, A. Chakraborty, H. Ohta, S. P. DenBaars, S. Nakamura, and J. S. Speck, Appl. Phys. Lett. **96**, 231912 (2010).
[24] C. F. Johnston, M. J. Kappers, and C. J. Humphreys, J. Appl. Phys. **105**, 073102 (2009).
[25] X. Ni, Ü. Özgür, Y. Fu, N. Biyikli, J. Xie, A. A. Baski, H. Morkoç, and Z. Liliental-Weber, Appl. Phys. Lett. **89**, 262105 (2006).